GEOPHYSICAL RESEARCH LETTERS, VOL. 34, L04310, doi:10.1029/2006GL028477, 2007

Postseismic deformation following the 1991 Racha, Georgia, earthquake

J. Podgorski,[1] E. H. Hearn,[1] S. McClusky,[2] R. Reilinger,[2] T. Taymaz,[3] O. Tan,[3,4] M. Prilepin,[5] T. Guseva,[5] and M. Nadariya[6]

Received 15 October 2006; accepted 13 December 2006; published 24 February 2007.

[1] The 1991, M_s = 7.0 Racha earthquake is the largest ever recorded in the Caucasus Mountains. Approximately three months after this thrust-faulting earthquake, a GPS network was set up to measure postseismic surface deformation. We present an analysis of these data, which indicate accelerated postseismic motions at several near-field sites. We model this deformation as either afterslip on the rupture surface or viscoelastic relaxation of the lower crust. We find that the postseismic motions are best explained by shallow afterslip on the earthquake rupture plane. The minimum postseismic moment release is estimated at 6.0×10^{18} N m, which is over 200 times the moment released by aftershocks in this same period and about 20% of the coseismic moment. We also show that the effective viscosity of the lower crust in the western Greater Caucasus region exceeds 10^{18} Pa s. **Citation:** Podgorski, J., E. H. Hearn, S. McClusky, R. Reilinger, T. Taymaz, O. Tan, M. Prilepin, T. Guseva, and M. Nadariya (2007), Postseismic deformation following the 1991 Racha, Georgia, earthquake, *Geophys. Res. Lett.*, *34*, L04310, doi:10.1029/2006GL028477.

1. Introduction

[2] The Greater Caucasus mountains mark the northernmost collisional boundary between the Arabian and Eurasian plates, forming a 1000 km long, WNW-ESE range between the Black and Caspian Seas (Figure 1). Approximately 10 mm/yr of roughly north-south convergence is accommodated by this range [*Reilinger et al.*, 2006]. On April 29, 1991, the Caucasus region was struck by its largest recorded earthquake: the M_s = 7.0 Racha earthquake [*Triep et al.*, 1995]. To characterize accelerated postseismic deformation, a GPS network was subsequently established [*Reilinger et al.*, 1997]. Here, we present an analysis of deformation recorded by this network, which was occupied five times between 1991 and 2001. We also develop models to test whether the observed postseismic deformation resulted from afterslip or viscoelastic relaxation of the thickened lower crust. It is our hope that our findings on lower crustal viscosity and the importance of aseismic fault slip will provide useful constraints for models of young continental collision and an improved picture of the extent to which aseismic deformation accommodates upper crustal shortening in this region.

2. GPS Network and Data Analysis

[3] Figure 1 shows locations of eight GPS stations in the vicinity of the Racha earthquake, where position measurements were made in five campaigns between the earthquake (April 29, 1991) and September, 2000. The dates of these site occupations are summarized in Table S1 of the auxiliary material.[1] The details of the GPS phase data processing strategy, error analysis and reference frame definitions used in this paper are given by *Reilinger et al.* [2006]. The station time series position estimates of the five Racha campaign solutions used here are realized by estimating a six-parameter transformation (three components of position translation and rotation), using the generalized constraints technique described by *Dong et al.* [1998]. Specifically, at each solution epoch we minimized (in a least squares sense) the differences in horizontal position estimates of between 16 to 44 GPS stations (see Table S1) with respect to the *Reilinger et al.* [2006] Eurasia fixed realization of the ITRF2000I [*Ray et al.*, 2004] reference frame. The median wrms fits of the horizontal position estimates used in the transformation estimation range from 4.2 mm in 1991 to 1.0 mm in 2000 (see Table S1).

2.1. GPS Time Series Analysis

[4] Position-time data (three components) from each GPS site were fit to simple linear, exponential, and logarithmic functions using the program TSVIEW [*Herring*, 2003].

$$x_{(t)} = x_0 + v(t - t_0) \tag{1}$$

$$x_{(t)} = x_0 + v(t - t_0) + \lambda \ln\left(1 + \frac{t - t_0}{\tau}\right) \tag{2}$$

$$x_{(t)} = x_0 + v(t - t_0 + \lambda)\left(1 - e^{-(t - t_0/\tau)}\right) \tag{3}$$

[5] In the above equations, t_0 is the time of the earthquake, x_0 is an offset at t = t_0, v is velocity, x is displacement, λ is the amplitude of the logarithmic or exponential term, and τ is a characteristic decay time. Misfit is quan-

[1]Department of Earth and Ocean Sciences, University of British Columbia, Vancouver, British Columbia, Canada.
[2]Department of Earth, Atmospheric, and Planetary Sciences, Massachusetts Institute of Technology, Cambridge, Massachusetts, USA.
[3]Department of Geophysics, Istanbul Technical University, Istanbul, Turkey.
[4]Now at TUBITAK Marmara Research Center, Earth and Marine Science Institute, Gebze, Kocaeli, Turkey.
[5]United Institute of Physics of the Earth, Moscow, Russia.
[6]Joint Stock Company Airgeodetic, Tbilisi, Georgia.

0094-8276/07/2006GL028477$05.00

[1]Auxiliary materials are available at ftp://ftp.agu.org/apend/gl/2006gl028477.

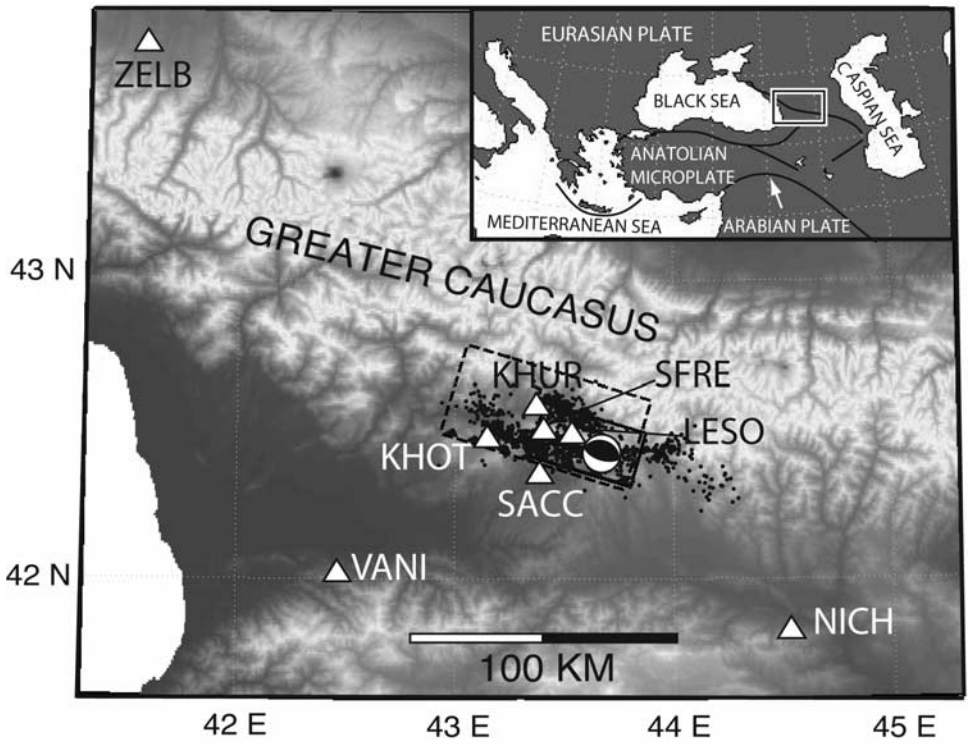

Figure 1. Location of the Racha rupture area and GPS stations (white triangles). Solid rectangle signifies the surface projection of the coseismic slip plane of *Tan and Taymaz* [2006]. Dashed rectangle marks the surface outline of the modeled afterslip plane in this paper. Both planes dip 30° to the NE.

tified as the weighted standard deviation (WSD). Values of WSD for each site are summarized in the auxiliary material, Table S2. At some GPS sites near the earthquake epicenter, the logarithmic function clearly fits the GPS position data better than the linear function, confirming that in the near field, a period of accelerated deformation followed the earthquake. The decay time of this transient is poorly constrained; for example, in the logarithmic case, varying the decay time between 1 and 100 days did not affect the WSD values. This is because of the three-year interval between the first two observations, and the large errors associated with the 1991 position measurements.

[6] Since exponential and logarithmic functions fit the data about equally well, we report the misfit measures for the logarithmic and linear functions only. Given that there is a change in GPS site velocities over the observation interval, but that its functional form is not well constrained, we model displacements separately over the 1991–1994 and 1994–1996 intervals.

2.2. Correction for Secular Deformation

[7] The Greater Caucasus region experiences north - south shortening of about 10 mm/yr [*Reilinger et al.*, 1997, 2006] leading to significant velocity gradients across the region covered by our network. This signal must be removed to isolate the postseismic deformation. In the absence of a GPS velocity field in the region prior to this 1991 earthquake, we have chosen two approaches. In the first approach, we assume that the postseismic transient is complete within about five years, as has been observed following other moderate to large continental thrust faulting earthquakes [e.g., *Donnellan and Lyzenga*, 1998; *Segall et al.*, 2000;

Table 1. GPS Postseismic Displacements for the 1991–1994 Time Period, With 1 - σ Errors

	Corrected With Time Series[a]			Corrected With Block Model[b]		
Site	North, mm	East, mm	Up, mm	North, mm	East, mm	Up, mm
KHOT	9.6 ± 9.8	20. ± 22.	40. ± 52	8.4 ± 6.1	21 ± 20.	60. ± 35
KHUR	−19 ± 8.0	9.5 ± 11.6	55 ± 44.	−22 ± 4.9	5.5 ± 6.5	69.7 ± 30.
LESO	−13 ± 4.4	−6.8 ± 6.6	82 ± 35	−20. ± 4.2	−4.2 ± 6.4	96 ± 29
NICH	no data	no data	no data	1.6 ± 3.2	−5.4 ± 3.6	88 ± 27
SACC	0.42 ± 8.9	6.0 ± 12.6	20. ± 42	7.0 ± 3.8	3.7 ± 5.7	42 ± 27
SFRE	−10. ± 8.9	−4.3 ± 12.4	64 ± 50	−5.8 ± 5.4	−5.8 ± 7.9	89 ± 32
VANI	4.2 ± 5.2	6.7 ± 6.0	32 ± 35	1.4 ± 3.1	9.3 ± 3.6	−8.6 ± 27
ZELB	0.54 ± 2.0	3.3 ± 3.2	51 ± 22	−0.78 ± 1.7	3.9 ± 2.5	70. ± 22

[a]Displacements are corrected for secular deformation using the 1996–2000 velocities for each GPS site.
[b]Displacements are corrected for secular deformation using velocities from the block model of *Reilinger et al.* [2006].

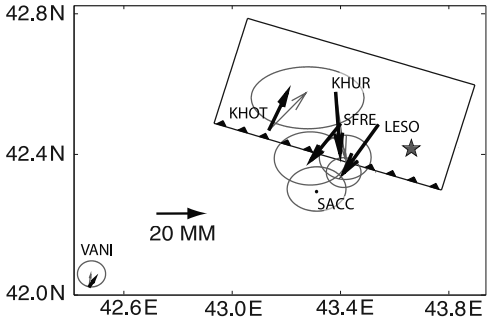

Figure 2. Displacement vectors for the 1991–1994 postseismic time period. Vectors with ellipses are time series-corrected displacements with 1 - σ errors. Bold vectors are the forward-modeled displacements, using fault slip from the afterslip inversion. The rectangle shows the surface projection of the fault segment on which we modeled afterslip, which dips to the northeast.

Hsu et al., 2002]. We estimate the velocity at each site from 1996 to 2000 and use this to correct the earlier displacement data. In the second approach, we use secular velocities from a block model of the region [*Reilinger et al.*, 2006] to correct the displacement data for 1991–1994 and 1994–1996 (the second period ends in 1996 so we can use both secular correction approaches). Secular velocities from the block model and from the 1996–2000 GPS position data are listed in Table S3 of the auxiliary material. Table 1 shows the corrected GPS site displacements for the 1991–1994 epoch, and Figure 2 shows the time series-corrected displacement vectors. Corrected displacements from the 1994–1996 epoch are included in Table S4 of the auxiliary material.

3. Modeling and Interpretation

[8] Postseismic deformation following large earthquakes has been attributed to aseismic slip driven by coseismic stresses [e.g., *Hearn et al.*, 2002], viscoelastic relaxation of lower crust or upper mantle layers with various linear and nonlinear rheologies [e.g., *Freed and Lin*, 1998], poroelastic effects [e.g., *Peltzer et al.*, 1998], or anelastic creep of the upper crust [*Donnellan and Lyzenga*, 1998], sometimes acting in combination. We model the Racha postseismic data for two simple end-member cases. For the first, we invert the displacements for slip on the earthquake rupture and surrounding parts of the same fault, assuming that elastic deformation in response to shear dislocations at depth causes the surface deformation [*Okada*, 1985; *Arnadottir and Segall*, 1994]. In these models we assume the Earth is a uniform, Poisson halfspace with a shear modulus (G) of 30 GPa. The fault plane geometry (strike = 287°, dip = 30°, with the hypocentre at 42.42° latitude 43.67° longitude, 6 km depth) is from *Tan and Taymaz* [2006], and is similar to that inferred by *Triep et al.* [1995] and *Fuenzalida et al.* [1997]. The model fault plane extends beyond that of *Tan and Taymaz* [2006] to permit afterslip both downdip and beyond the ends of the coseismic rupture. In the second case we forward model viscoelastic relaxation for a variety of lower crust or upper mantle viscosity structures using the semi-analytical code VISCO1D [*Pollitz*, 1997]. For both classes of models we compute the WRSS (weighted residual sum of squares) summed for all three degrees of freedom (east, north, and up) for all of the GPS sites, and minimize this quantity to identify the best afterslip distribution or viscosity structure (that is, relaxing layer thickness and effective viscosity). Displacements over two time intervals are modeled and discussed separately.

[9] Resolution tests suggest that the GPS network can only resolve afterslip in the hypocentral region and to the west, so this is all we show on Figures 1, 2, and 3. Using the 1991–1994 displacements, corrected for secular deformation using both approaches described above, we find similar patterns of shallow afterslip (Figure 3). The afterslip in both cases is concentrated at depths of 0 to 4 km, though another high afterslip patch downdip (at a depth of 12 km, located 40 km west of the hypocentre) is also apparent. A cross-validation sum of squares (CVSS) analysis shows that the deeper slip patch is required principally by the displacement of GPS site KHUR. The total afterslip moment release is 6 to 7.6 $\times$ 10^{18} N m, or 19 to 24% of the coseismic moment (3.2 $\times$ 10^{19} N m [*Tan and Taymaz*, 2006]). The aftershock

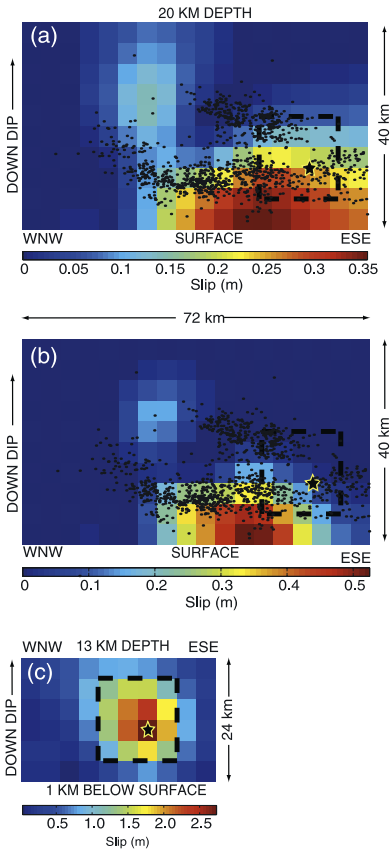

Figure 3. Coseismic slip and modeled afterslip between 1991 and 1994 (in meters). (a) Afterslip inversion result using GPS site displacements corrected for secular deformation with 1996–2000 velocities. (b) Afterslip inversion result using GPS site displacements corrected with a block model [*Reilinger et al.*, 2006]. (c) Coseismic slip model of *Tan and Taymaz* [2006]. The fault plane of afterslip models shown in Figures 3a and 3b is an extended version of the plane from the coseismic slip model shown in Figure 3c. The star represents the Racha earthquake hypocenter.

moment release in this region (42.2988–42.7871°N latitude and 42.9330–43.8961°E longitude) over the same time interval (based on the Harvard CMT catalogue and the aftershock data from *Fuenzalida et al.* [1997]) is 2.4×10^{16} N m, or 0.08% of the coseismic moment. The afterslip seems to occur in regions where aftershocks are absent, and most of the afterslip is just updip of the coseismic rupture, where shear stresses on the fault were increased by the earthquake. The afterslip models are associated with WRSS values that are 90% and 66% lower than values that would result from a model with stationary GPS sites. We also found that the slip distribution and WRSS are insensitive to small variations in slip plane geometry (i.e. within the range of published values). Models of the later (1994–1996) GPS site displacements show that afterslip reduces the WRSS for this time interval by only 22 to 25% relative to a model with stationary GPS sites.

[10] For the viscoelastic models, we vary the thickness and the effective viscosity of a relaxing lower crustal layer. We fix the base of the lower crust at 45 km [*Philip et al.*, 1989; *Ruppel and McNutt*, 1990] and vary the lower crustal thickness from 10 to 30 km (hence varying the plate thickness as well). Effective viscosities between 10^{17} and 10^{20} Pa s were investigated. The best viscoelastic model calls for a lower crustal viscosity of 9.0×10^{17} Pa s over the depth interval 25 to 45 km. However, this model reduces the WRSS by just 21% relative to a model in which GPS sites are stationary. For the 1994 to 1996 epoch, this viscoelastic model yields a larger WRSS than a model with stationary GPS sites.

4. Discussion and Conclusions

[11] Our models of postseismic deformation following the 1991 Racha, Georgia, earthquake suggest that significant afterslip followed this event, while contributions from viscoelastic relaxation of the lower crust were minor or absent. Unlike *Reilinger et al.* [1997], we find predominantly shallow afterslip (i.e., within the top few kilometers of the crust). This is compatible with velocity-strengthening friction, which promotes aseismic slip, in the top few kilometers of the crust [*Marone et al.*, 1991]. We may underestimate the total moment of afterslip because (1) we cannot resolve slip east of the hypocentre with data from this GPS network and (2) the GPS network was not installed until about 87 days after the earthquake. On the other hand, our treating the domain as an elastic halfspace for the slip inversion neglects a contrast in properties across the fault, with a lower-strength material in the hanging wall, where most of the GPS sites are located. This will cause us to slightly overestimate the coseismic slip where we were able to resolve it. Afterslip appears to have ceased (or slowed significantly) by 1994. The duration and relative moment of Racha afterslip are comparable to values from other reverse faulting earthquakes observed by GPS [e.g., *Donnellan and Lyzenga*, 1998; *Hsu et al.*, 2002; *Segall et al.*, 2000]. We also note that local plastic deformation, such as that suggested for the Northridge earthquake [*Donnellan and Lyzenga*, 1998], cannot be ruled out.

[12] Seismic estimates of convergence across the Main Caucasus Thrust (MCT) vary substantially, but are generally less than both geologic and geodetic estimates [*Philip et al.*, 1989; *Jackson*, 1992; *Reilinger et al.*, 1997]. *Jackson* [1992] includes the Racha earthquake in his seismic estimate of convergence rate and reports a maximum rate of about 4 mm/yr, with a preferred rate of 3.4 mm/yr, for the entire MCT. In the east (that is, east of where the Borzhomi-Kazbeg fault zone crosses the MCT), this is only about 30% of the geodetic convergence rate. In the western part of the Greater Caucasus, where the Racha earthquake occurred, however, this rate is close to the GPS rate from the kinematic model of *Reilinger et al.* [2006] block model (3.0 ± 0.2 mm/yr). Given the modest but non-negligible afterslip that we have observed and the similarity of GPS and seismic slip rates for the western part of the MCT, most convergence in this area is accommodated by earthquakes in the upper crust.

[13] If viscoelastic relaxation of the lower crust followed the Racha earthquake, it was at too low a rate to be captured with this GPS network. The dominance of afterslip between 1991 and 1994, and GPS constraints on the upper limit of surface displacements between 1994 and 1996, require a lower crustal viscosity (25–45 km) of at least 10^{18} Pa s. Assuming a temperature gradient of 20 degrees per km, typical wet quartz flow laws [e.g., *Gleason and Tullis*, 1995] may be ruled out for the lower crust. A somewhat higher effective viscosity would still be consistent with low seismic velocities [*Hearn and Ni*, 1994] and high attenuation [*Kadinski-Cade et al.*, 1981; *Sarker and Abers*, 1998; *Sandvol et al.*, 2001] in the thickened, Caucasus lower crust. However, recent modeling studies of young continental collision zones have assumed extremely weak lower crust (for example, 25% of values given by *Gleason and Tullis* [1995], by *Pysklywec et al.* [2002]) to decouple the mantle lithosphere from the upper crust. If such low values can be ruled out then models with more coupled crust and mantle [e.g., *Beaumont et al.*, 1996] may be more applicable to the Caucasus collision zone.

[14] **Acknowledgments.** This research was funded in part by an NSERC Discovery grant to UBC, and by NSF grant EAR-0337497 to MIT.

References

Arnadottir, T., and P. Segall (1994), The 1989 Loma Prieta earthquake imaged from inversion of geodetic data, *J. Geophys. Res.*, *99*, 21,835–21,855.

Beaumont, C., P. J. J. Kamp, J. Hamilton, and P. Fullsack (1996), The continental collision zone, South Island, New Zealand: Comparison of geodynamical models and observations, *J. Geophys. Res.*, *101*, 3333–3360.

Dong, D., T. A. Herring, and R. W. King (1998), Estimating regional deformation from a combination of space and terrestrial geodetic data, *J. Geod.*, *72*, 200–214.

Donnellan, A., and G. A. Lyzenga (1998), GPS observations of fault afterslip and upper crustal deformation following the Northridge earthquake, *J. Geophys. Res.*, *103*, 21,285–21,297.

Freed, A. M., and J. Lin (1998), Time-dependent changes in failure stress following thrust earthquakes, *J. Geophys. Res.*, *103*, 24,393–24,410.

Fuenzalida, H., L. Rivera, H. Haessler, D. Legrand, H. Philip, L. Dorbath, D. McCormack, S. Arefiev, C. Langer, and A. Cisternas (1997), Seismic source study of the Racha-Dzhava (Georgia) earthquake from aftershocks and broadband teleseismic body-wave records: An example of active nappe tectonics, *Geophys. J. Int.*, *130*, 29–46.

Gleason, G. C., and J. Tullis (1995), A flow law for dislocation creep of quartz aggregates determined with the molten salt cell, *Tectonophysics*, *247*, 1–23.

Hearn, E. H., R. Burgmann, and R. E. Reilinger (2002), Dynamics of Izmit earthquake postseismic deformation and loading of the Duzce earthquake hypocenter, *Bull. Seismol. Soc. Am.*, *92*, 172–193.

Hearn, T., and J. Ni (1994), *Pn* velocities beneath continental collision zones: The Turkish-Iranian Plateau, *Geophys. J. Int.*, *117*, 273–283.

Herring, T. (2003), MATLAB tools for viewing GPS velocities and time series, *GPS Solutions*, *7*, 194–199.

Hsu, Y.-J., N. Bechor, P. Segall, S.-B. Yu, L.-C. Kuo, and K.-F. Ma (2002), Rapid afterslip following the 1999 Chi-Chi, Taiwan earthquake, *Geophys. Res. Lett.*, *29*(16), 1754, doi:10.1029/2002GL014967.

Jackson, J. (1992), Partitioning of strike-slip and convergent motion between Eurasia and Arabia in eastern Turkey and the Caucasus, *J. Geophys. Res.*, *97*, 12,471–12,479.

Kadinski-Cade, K., M. Barazangi, J. Oliver, and B. Isacks (1981), Lateral variations in high frequency seismic wave propagation at regional distances across the Turkish and Iranian Plateaus, *J. Geophys. Res.*, *86*, 9377–9396.

Marone, C. J., C. H. Scholz, and R. Bilham (1991), On the mechanics of earthquake afterslip, *J. Geophys. Res.*, *96*, 8441–8452.

Okada, Y. (1985), Surface deformation due to shear and tensile faults in a half-space, *Bull. Seismol. Soc. Am.*, *75*, 1135–1154.

Peltzer, G., P. Rosen, F. Rogez, and K. Hudnut (1998), Poroelastic rebound along the Landers 1992 earthquake surface rupture, *J. Geophys. Res.*, *103*, 30,131–30,146.

Philip, H., A. Cisternas, A. Gvishani, and A. Gorshkov (1989), The Caucasus: An actual example of the initial stages of continental collision, *Tectonophysics*, *161*, 1–21.

Pollitz, F. F. (1997), Gravitational viscoelastic postseismic relaxation on a layered spherical Earth, *J. Geophys. Res.*, *102*, 17,921–17,941.

Pysklywec, R. N., C. Beaumont, and P. Fullsack (2002), Lithospheric deformation during the early stages of continental collision: Numerical experiments and comparison with South Island, New Zealand, *J. Geophys. Res.*, *107*(B7), 2133, doi:10.1029/2001JB000252.

Ray, J., D. Dong, and Z. Altamimi (2004), IGS reference frames: Status and future improvements, paper presented at IGS 2004 Workshop, Astron. Inst., Berne, 1–5 Mar.

Reilinger, R. E., S. C. McClusky, B. J. Souter, M. W. Hamburger, M. T. Prilepin, A. Mishin, T. Guseva, and S. Balassanian (1997), Preliminary estimates of plate convergence in the Caucasus collision zone from global positioning system measurements, *Geophys. Res. Lett.*, *24*, 1815–1818.

Reilinger, R., et al. (2006), GPS constraints on continental deformation in the Africa-Arabia-Eurasia continental collision zone and implications for the dynamics of plate interactions, *J. Geophys. Res.*, *111*, B05411, doi:10.1029/2005JB004051.

Ruppel, C., and M. McNutt (1990), Regional compensation of the Greater Caucasus mountains based on an analysis of Bouguer gravity data, *Earth Planet. Sci. Lett.*, *98*, 360–379.

Sandvol, E., K. Al-Damegh, A. Calvert, D. Seber, M. Barazangi, R. Mohamad, R. Gok, N. Turkelli, and C. Gurbuz (2001), Tomographic imaging of the *Lg* and *Sn* propagation in the Middle East, *Pure Appl. Geophys.*, *158*, 1121–1163.

Sarker, G., and G. A. Abers (1998), Deep structures along the boundary of a collisional belt: Attenuation tomography of *P* and *S* waves in the Greater Caucasus, *Geophys. J. Int.*, *133*, 326–340.

Segall, P., R. Burgmann, and M. Matthews (2000), Time-dependent triggered afterslip following the 1989 Loma Prieta earthquake, *J. Geophys. Res.*, *105*, 5615–5634.

Tan, O., and T. Taymaz (2006), Active tectonics of the Caucasus: Earthquake source mechanisms and rupture histories obtained from inversion of teleseismic body waveforms, in *Postcollisional Tectonics and Magmatism in the Mediterranean Region and Asia*, edited by Y. Dilek and S. Pavlides, *Spec. Pap. Geol. Soc. Am.*, *409*, 531–578.

Triep, E. G., G. A. Abers, A. L. Lerner-Lam, V. Mishatkin, N. Zakharchenko, and O. Starovoit (1995), Active thrust front of the Greater Caucasus: The April 29, 1991 Racha earthquake sequence and its tectonic implications, *J. Geophys. Res.*, *100*, 4011–4033.

T. Guseva and M. Prilepin, United Institute of Physics of the Earth, Russian Academy of Sciences, B. Gruzinskaya 10, Moscow 143810, Russia. (strakhov@dir.iephys.msk.su; prilepin@uipe-ras.scgis.ru)

E. Hearn and J. Podgorski, Department of Earth and Ocean Sciences, University of British Columbia, 6339 Stores Road, Vancouver, BC, Canada V6S 1R6. (ehearn@eos.ubc.ca; jpodgorski@eos.ubc.ca)

S. McClusky and R. Reilinger, Department of Earth, Atmospheric, and Planetary Sciences, Massachusetts Institute of Technology, 42 Carleton Street, Cambridge, MA 02139, USA. (simon@chandler.mit.edu; reilinge@erl.mit.edu)

M. Nadariya, Joint Stock Company Airgeodetic, Tbilisi, Georgia.

O. Tan, TUBITAK Marmara Research Center, Earth and Marine Science Institute, Gebze, Kocaeli, Turkey. (onur.tan@mam.gov.tr)

T. Taymaz, Department of Geophysical Engineering, Istanbul Technical University, Maslak, Istanbul TR-34390, Turkey. (taymaz@itu.edu.tr)